Dual-stage Model Predictive Control Based Reduced Model Framework for Voltage Control in Active Distribution Networks

Mudaser Rahman Dar, *Graduate Student Member*, *IEEE* and Sanjib Ganguly, *Senior Member*, *IEEE*

***Abstract*—The large-scale penetration of photovoltaic (PV) units and controllable loads such as electric vehicles (EVs) render the distribution networks prone to frequent, uncertain, and simultaneous over/under voltages. The coordinated control of devices such as on-load tap changer (OLTC), PV inverters, and EV chargers seem efficient in regulating the distribution network voltage within normal operation limits. However, the need for measuring infrastructure throughout the distribution network and communication setup to all control devices makes it practically and economically difficult. Furthermore, for large networks, the large measurement dataset of the network and distributed control resources increase the computational complexity and the response time. This paper proposes a voltage control strategy based on dual-stage model predictive control by coordinating devices such as OLTC and controllable PVs and EV charging stations. A minimum set of available control resources is identified to establish the voltage control in the network with reduced communication and minimum measuring infrastructure, using a reduced model framework. Simulations are performed on 33-bus distribution network and the modified IEEE 123-bus distribution network to validate the efficacy of the proposed control strategy.**

***Index Terms*—Active distribution network, distributed generation, photovoltaic (PV), model predictive control (MPC).**

I. Introduction

THE widespread integration of distributed energy resources (DERs) notably in last decades has turned traditional passive power distribution networks into active distribution networks (ADNs). The integration of DERs, mainly photovoltaic (PV) units, increases network flexibility, operation cost, and sustainability. However, it may also lead to unstable and insecure operations due to reverse power flow, simultaneous over/under voltages, and other power quality complications [1], [2]. The deployment of DERs such as wind turbines and PV sources along with controllable loads such as electric vehicles (EVs) further exacerbates the active network management (ANM) due to the uncertainties associated with them in spatio-temporal distribution [3]. To make the distribution networks resilient to the technical challenges raised by high integration of DERs, enhanced monitoring and control become significantly important. The control capabilities of DERs and other control devices along with enhanced communication and measurement infrastructure promise the stable operation of ADNs to avoid or at least postpone network reinforcement [4].

The voltage rise problem forms one of the prominent issues in ADNs. Over the years, a large number of research works have been carried out for real-time voltage and reactive power control so as to deal with uncertain and frequent voltage violations. The volt/var optimization (VVO) is a critical feature of ANM, wherein the control capabilities of fast-acting devices such as PV and EV inverters, storage devices, and other power electronic interfaced devices such as soft open point (SOP), are utilized for the voltage regulation and loss minimization [5]. Over the years, various voltage control strategies have been proposed for voltage control and VVO in ADNs, which can be broadly classified as local/decentralized, centralized, distributed, and hybrid voltage controls. Local control forms the simplest voltage control strategy, wherein control actions are taken based on pre-specified rules and local measurements [6] - [8]. Local control strategies lack optimization or coordination among resources, thus are suited for networks with limited control resources.

Centralized control is widely studied in small/medium distribution networks, owing to their rule-based or optimization-based coordination among control resources [9]. Optimization-based coordination has been carried out on single-time-scale coordination [1], [3], [5], [10] - [12] and multi-time-scale coordination [13]-[15], wherein the devices with different temporal operation characteristics are coordinated at different time scales. Most of the research works anticipate the uncertain generation from RESs such as PVs, thus avoiding the necessary uncertainties. References [5], [16]-[18] have incorporated randomness and uncertainties in generation and load using techniques such as stochastic programming. Reference [16] considers random stochasticity in EV charging and discharging, and [17] accounts for uncertainties by considering worst-case transitions in stochastic resources for voltage control using robust constrained model predictive control (RC-MPC). The uncertainty in line parameters is considered in [18] while regulating node voltages. The need for reliable

Manuscript received: April 12, 2024; revised: May 23, 2024; accepted: June 3, 2024. Date of CrossCheck: June 3, 2024. Date of online publication: June 21, 2024.

M. R. Dar and S. Ganguly (corresponding author) are with the Department of Electronics and Electrical Engineering, Indian Institute of Technology, Guwahati, India (e-mail: m.dar@iitg.ac.in; sanjib191@gmail.com).

DOI: 10.35833/MPCE.2024.000394

communication, information transparency, and complexity in control makes it difficult for centralized control strategies in large distribution networks. To account for heavy communication and the need for voltage control in large distribution networks, distributed voltage control seems to be promising, wherein various distributed controllers coordinate with communication among neighboring controllers. Distributed coordinated control is carried out using multi-agent system-based coordination algorithms [19], [20], decomposition coordination-based algorithms [21]-[23], and consensus-based algorithms [24]-[26]. However, distributed control strategies are technically difficult to implement.

Recently, hybrid control strategies have been used to regulate voltage efficiently by hybridizing and utilizing the merits of centralized, local, and distributed control strategies [4], [27]-[29]. Furthermore, to account for the need for system models, deep learning-based voltage control strategies are gaining interest [30]-[32], using the coordination of the above-mentioned strategies.

Recent years have seen a significant rise in predictive control, notably model predictive control (MPC), driven by the abundance of data logs and enhanced by recent advances in short-term forecasting. MPC employs a system model for iterative computation of control variables at each control step and strategically optimizes the anticipated future behavior of the underlying system.

Within the existing literature, studies exploring MPC-driven voltage control have been investigated within local [33], decentralized [34], centralized [10]-[15], as well as distributed [35]-[37] frameworks. Centralized MPC-based strategies are relatively easier to implement than distributed control strategies, for small and medium-sized networks. In [11]-[13], [15], the active/reactive power exchange leveraging smart inverters is used along with an on-load tap changer (OLTC); however, the measurements are assumed to be available from every node, so that the controller apprehends the system state for real-time control. Moreover, all control resources are utilized increasing the communication burden. A distributed solution is proposed in [36] with optimality features of centralized control. However, in a distributed setting, the full set of network measurements is needed. Using diverse control equipment, [37] proposes a distributed MPC-based control strategy employing the gradient projection method to find the optimal solution. A decentralized control strategy utilizing coordination among different clusters is proposed in [34]. The control strategy mitigates the communication requirements, while no attention is given to the optimality of solution compared with centralized strategies. Since centralized control demands extensive two-way communication with each controllable device, scaling this centralized strategy becomes cost-prohibitive with the increasing number of control devices. Distributed control strategies offer a viable alternative that requires sparse communication, but optimal solutions may not be always guaranteed. Moreover, in future distribution networks with highly penetrated distributed generation (DG) units and EVs, the coordination of all control resources with different temporal characteristics will increase the complexities of computation and coordination.

To this end, this paper proposes a voltage control strategy leveraging a dual-stage MPC-based reduced model framework that requires less network information, communication, and control needs, thus encompassing the benefits of both distributed and centralized control structures discussed above. A dual-stage MPC is used in [13] to coordinate control devices with different temporal characteristics; however, the measuring infrastructure is assumed to be installed throughout the network and all control resources are used for voltage regulation. Reference [14] has carried out MPC-based real-time voltage control in ADNs in which the need for measuring infrastructure throughout the network is reduced. However, all the control resources available in the network are monitored and used for voltage regulation. Furthermore, the MPC framework is single-stage designed for the coordination of only fast-acting control resources such as DG units and energy storage systems (ESSs). Reference [38] proposes an index for identifying the most effective control resources for voltage regulation. However, for the identification of the nodes with voltage violations, it is required to monitor all nodes in the network. Furthermore, for different voltage violation cases, different sets of effective control resources are needed, which requires the availability of all control resources. Hence, to address these research gaps, this paper presents a real-time voltage control strategy in ADNs based on dual-stage MPC with a reduced model framework. A comparison of existing control strategies with this paper is drawn in Table I.

TABLE I
COMPARISON OF EXISTING CONTROL STRATEGIES WITH THIS PAPER

Reference	Control strategy	Reduced number of sensors and measuring infrastructure	Reduced number of control resources
[13]	Dual-stage MPC	×	×
[14]	Single-stage MPC	√	×
[38]	Index-based	×	√
This paper	Dual-stage MPC	√	√

A minimum measuring infrastructure and a global minimum set of available control resources for voltage regulation are used throughout the network. The critical nodes for measurements are identified using the network partitioning based on hierarchical clustering algorithm (HCA) [39]. A global set of control resources is identified by ranking the control resources using numerical voltage sensitivity analysis, to provide a reduced model framework and bring down the number of sensors and measuring devices as well as communication infrastructure. The reduced model framework highly reduces the computational complexity and response time of the controller. It is to be noted that a system model is imperative for employing MPC; however, a distribution network model is rarely available. Existing literature commonly assumes the availability of the network model, and thus extracts the necessary parameters such as voltage sensitivity coefficients from Newton-Raphson (NR) power flow [4], [10], [13] or other analytical methods [14], [17], relying on

known line parameters. In case the network model is not available, the sensitivities can be extracted experimentally if the measurements are available throughout the network. However, the proposed control strategy, featuring a reduced model structure, demands sensitivity coefficients for selected nodes (control and observation nodes) only. These required nodal sensitivities can be experimentally computed using measured-data-based sensitivity calculation methods as in [40], [41], with the limited number of devices present. Thus, the main objectives of this paper can be summarized as follows.

1) Development of dual-stage MPC-based reduced model framework for voltage control in ADNs with control devices of different temporal characteristics.

2) Network partitioning to identify critical nodes for measurements (termed as observation nodes) and ranking of available control resources using novel ranking index (*RI*), by utilizing numerical voltage sensitivity analysis.

3) Identification of global control resource set among the ranked control resources and implementation of the MPC-based control strategy on the 33-bus distribution network and modified IEEE 123-bus distribution network in simulation.

The remainder of the paper is organized as follows. Section II provides the dual-stage MPC. Section III discusses the optimization problem formulation. Section IV formulates the reduced model framework, with reduced measurement and communication infrastructure and reduced use of control resources. Section V presents the modeling and description of the test distribution networks. Section VI presents the simulation results on the IEEE 33-bus distribution network and modified IEEE 123-bus distribution network with the proposed control strategy and discussions. Finally, Section VII provides the conclusion of this paper.

II. Dual-stage MPC

MPC efficaciously deals with complex dynamic systems to predict the system behavior. MPC employs the system model and current system state to determine the optimal control sequence over multiple time steps called control horizon N_c. The system behavior is predicted based on optimal control sequence over the prediction horizon N_p. The system evolution is depicted in Fig. 1.

The system is expressed by a discrete linear model [42] as:

$$\boldsymbol{z}(k+1)=\hat{\boldsymbol{A}}\boldsymbol{z}(k)+\hat{\boldsymbol{B}}\Delta\boldsymbol{u}(k) \tag{1}$$

$$\boldsymbol{y}(k)=\hat{\boldsymbol{C}}\boldsymbol{z}(k) \tag{2}$$

where $\hat{\boldsymbol{A}}$ and $\hat{\boldsymbol{B}}$ are the system matrix and input matrix, respectively; $\hat{\boldsymbol{C}}=[\hat{\boldsymbol{C}}_1^{\mathrm{T}}, \hat{\boldsymbol{C}}_2^{\mathrm{T}}]^{\mathrm{T}}$ is the output matrix corresponding to system output $\boldsymbol{y}(k)=[\boldsymbol{y}_1^{\mathrm{T}}(k), \boldsymbol{y}_2^{\mathrm{T}}(k)]^{\mathrm{T}}$; $\boldsymbol{z}$ is the state vector; $\Delta\boldsymbol{u}$ is the control input vector; and k is the time step. The system evolution is governed by a linear model given in (3) and (4), where $\delta\boldsymbol{v}/\delta\boldsymbol{u}$ and $\delta\boldsymbol{i}/\delta\boldsymbol{u}$ are the voltage ($\boldsymbol{v}$) sensitivity and current ($\boldsymbol{i}$) sensitivity to the control input $\boldsymbol{u}$ (OLTC tap change, active/reactive power exchange by PV inverters and EV charging stations (EVCSs)), respectively.

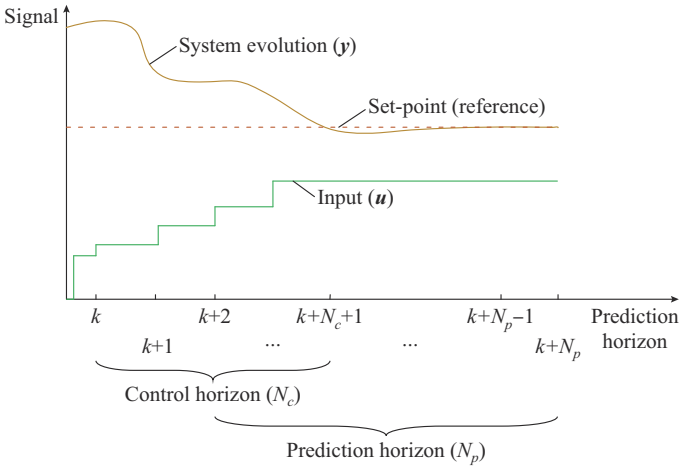

Fig. 1. MPC-based system evolution over prediction horizon.

$$\boldsymbol{v}(k+l)=\boldsymbol{v}(k+l-1)+\frac{\delta\boldsymbol{v}}{\delta\boldsymbol{u}}\Delta\boldsymbol{u}(k+l-1) \tag{3}$$

$$\boldsymbol{i}(k+l)=\boldsymbol{i}(k+l-1)+\frac{\delta\boldsymbol{i}}{\delta\boldsymbol{u}}\Delta\boldsymbol{u}(k+i-1) \tag{4}$$

Vectors $\boldsymbol{z}$ and $\boldsymbol{y}=[\boldsymbol{y}_1^{\mathrm{T}}, \boldsymbol{y}_2^{\mathrm{T}}]^{\mathrm{T}}$ represent the node voltages $\boldsymbol{y}_1$ and line currents $\boldsymbol{y}_2$, and $\Delta\boldsymbol{u}$ represents the change in active and reactive power at control nodes or change in voltage due to tap operation of OLTC. $\hat{\boldsymbol{B}}$ represents the sensitivities of monitored variables with respect to control variables. The voltage sensitivity coefficients can be obtained using analytical voltage sensitivity analysis to power flow equations [43], or can be extracted from numerical techniques such as Newton-Raphson (NR) power flow. In this paper, the voltage sensitivity coefficients are extracted from the inverse of the Jacobian matrix using the offline NR load flow method, and sensitivities of the branch currents are calculated at each sampling instant [13]. Sensitivities with respect to tap operations of OLTC are obtained by calculating deviations due to two successive tap operations. Based on the linearized discrete model of the system, the state variables are obtained sequentially over N_p as:

$$\begin{cases}\boldsymbol{z}(k+1|k)=\hat{\boldsymbol{A}}\boldsymbol{z}(k)+\hat{\boldsymbol{B}}\Delta\boldsymbol{u}(k)\\ \boldsymbol{z}(k+2|k)=\hat{\boldsymbol{A}}^2\boldsymbol{z}(k)+\hat{\boldsymbol{A}}\hat{\boldsymbol{B}}\Delta\boldsymbol{u}(k)+\hat{\boldsymbol{B}}\Delta\boldsymbol{u}(k+1)\\ \vdots\\ \boldsymbol{z}(k+N_p|k)=\hat{\boldsymbol{A}}^{N_p}\boldsymbol{z}(k)+\hat{\boldsymbol{A}}^{N_p-1}\hat{\boldsymbol{B}}\Delta\boldsymbol{u}(k)+\ldots+\hat{\boldsymbol{A}}^{N_p-N_c}\hat{\boldsymbol{B}}\Delta\boldsymbol{u}(k+N_c-1)\end{cases} \tag{5}$$

Using the above-obtained states, the predicted output can be obtained as:

$$\begin{cases}\boldsymbol{y}(k+1|k)=\hat{\boldsymbol{C}}\hat{\boldsymbol{A}}\boldsymbol{z}(k)+\hat{\boldsymbol{C}}\hat{\boldsymbol{B}}\Delta\boldsymbol{u}(k)\\ \boldsymbol{y}(k+2|k)=\hat{\boldsymbol{C}}\hat{\boldsymbol{A}}^2\boldsymbol{z}(k)+\hat{\boldsymbol{C}}\hat{\boldsymbol{A}}\hat{\boldsymbol{B}}\Delta\boldsymbol{u}(k)+\hat{\boldsymbol{C}}\hat{\boldsymbol{B}}\Delta\boldsymbol{u}(k+1)\\ \vdots\\ \boldsymbol{y}(k+N_p|k)=\hat{\boldsymbol{C}}\hat{\boldsymbol{A}}^{N_p}\boldsymbol{z}(k)+\hat{\boldsymbol{C}}\hat{\boldsymbol{A}}^{N_p-1}\hat{\boldsymbol{B}}\Delta\boldsymbol{u}(k)+\ldots+\\ \qquad\hat{\boldsymbol{C}}\hat{\boldsymbol{A}}^{N_p-N_c}\hat{\boldsymbol{B}}\Delta\boldsymbol{u}(k+N_c-1)\end{cases} \tag{6}$$

The control sequence over the control horizon $\Delta\boldsymbol{U}$ and the consequent predicted output sequence over the prediction horizon $\boldsymbol{Y}$ are represented by (7) and (8), respectively. It is to

be mentioned that only first control actions are applied using receding horizon control, to consider the system state at each optimization stage. Incorporating fresh measurements at each step alleviates the model inaccuracies (if any).

$$\Delta \boldsymbol{U}=[\Delta \boldsymbol{u}(k)^{\mathrm{T}}\ \Delta \boldsymbol{u}(k+1)^{\mathrm{T}}\ \Delta \boldsymbol{u}(k+N_c-1)^{\mathrm{T}}]^{\mathrm{T}} \tag{7}$$

$$\boldsymbol{Y}=[\boldsymbol{y}(k+1|k)^{\mathrm{T}}\ \boldsymbol{y}(k+2|k)^{\mathrm{T}}\ \boldsymbol{y}(k+N_p|k)^{\mathrm{T}}]^{\mathrm{T}} \tag{8}$$

The predicted output over the predicted horizon N_p can be expressed in terms of measurements and optimal inputs over the control horizon N_c as:

$$\boldsymbol{Y}=\hat{\boldsymbol{F}}\boldsymbol{z}(k)+\hat{\boldsymbol{\Phi}}\Delta \boldsymbol{U} \tag{9}$$

$$\hat{\boldsymbol{F}}=[(\hat{\boldsymbol{C}}\hat{\boldsymbol{A}})^{\mathrm{T}}\quad(\hat{\boldsymbol{C}}\hat{\boldsymbol{A}}^{2})^{\mathrm{T}}\quad(\hat{\boldsymbol{C}}\hat{\boldsymbol{A}}^{3})^{\mathrm{T}}\quad\ldots\quad(\hat{\boldsymbol{C}}\hat{\boldsymbol{A}}^{N_p})^{\mathrm{T}}]^{\mathrm{T}} \tag{10}$$

$$\hat{\boldsymbol{\Phi}}=\begin{bmatrix}\hat{\boldsymbol{C}}\hat{\boldsymbol{B}} & 0 & \ldots & 0\\ \hat{\boldsymbol{C}}\hat{\boldsymbol{A}}\hat{\boldsymbol{B}} & \hat{\boldsymbol{C}}\hat{\boldsymbol{B}} & \ldots & 0\\ \hat{\boldsymbol{C}}\hat{\boldsymbol{A}}^{2}\hat{\boldsymbol{B}} & \hat{\boldsymbol{C}}\hat{\boldsymbol{A}}\hat{\boldsymbol{B}} & \ldots & 0\\ \vdots & \vdots & & \vdots\\ \hat{\boldsymbol{C}}\hat{\boldsymbol{A}}^{N_p-1}\hat{\boldsymbol{B}} & \hat{\boldsymbol{C}}\hat{\boldsymbol{A}}^{N_p-2}\hat{\boldsymbol{B}} & \ldots & \hat{\boldsymbol{C}}\hat{\boldsymbol{A}}^{N_p-N_c}\hat{\boldsymbol{B}}\end{bmatrix} \tag{11}$$

The system state vector $\boldsymbol{z}(k)$ is acquired through real-time measurements at time step k. The output is predicted based on the change in control inputs. To obtain the control inputs at time step k, we can write:

$$\begin{cases}\boldsymbol{u}(k)=\boldsymbol{u}(k-1)+\Delta \boldsymbol{u}(k)\\ \boldsymbol{u}(k+1)=\boldsymbol{u}(k-1)+\Delta \boldsymbol{u}(k)+\Delta \boldsymbol{u}(k+1)\\ \vdots\\ \boldsymbol{u}(k+N_c-1)=\boldsymbol{u}(k-1)+\Delta \boldsymbol{u}(k)++\Delta \boldsymbol{u}(k+N_c-1)\end{cases} \tag{12}$$

Equation (12) reduces to the compact form:

$$\boldsymbol{U}(k)=\hat{\boldsymbol{G}}\boldsymbol{u}(k-1)+\hat{\boldsymbol{\Lambda}}\Delta \boldsymbol{U} \tag{13}$$

$$\begin{cases}\hat{\boldsymbol{G}}=[\boldsymbol{I}\ \ \boldsymbol{I}\ \ \ldots\ \ \boldsymbol{I}]^{\mathrm{T}}\\ \hat{\boldsymbol{\Lambda}}=\begin{bmatrix}\boldsymbol{I} & \boldsymbol{0} & \boldsymbol{0} & \ldots & \boldsymbol{0}\\ \boldsymbol{I} & \boldsymbol{I} & \boldsymbol{0} & \ldots & \boldsymbol{0}\\ \vdots & \vdots & \vdots & & \vdots\\ \boldsymbol{I} & \boldsymbol{I} & \boldsymbol{I} & \ldots & \boldsymbol{I}\end{bmatrix}\end{cases} \tag{14}$$

The previous input $\boldsymbol{u}(k-1)$ cumulatively adds all previous input changes in (12), thus the input changes at the previous time steps such as $\{\Delta \boldsymbol{u}(k-1),\Delta \boldsymbol{u}(k-2)\}$ are implicitly considered by the value of $\boldsymbol{u}(k-1)$. The voltage control architecture in ADNs is shown in Fig. 2.

It is worth mentioning that the choice of control horizon and prediction horizon involves a trade-off between computational complexity and rigorousness of the controller actions. The control action is taken such that the output meets the set point target at the end of the prediction horizon [10], as shown in Fig. 1. Since it is assumed that the measurements are available quite frequently due to advanced metering infrastructure, the control action is determined over a short time window. For this purpose, the prediction horizon is considered to be 3 (which is relatively low), so that the controller action is more aggressive than spreading the control action over a long time window. From the computational perspective, the prediction horizon is chosen to be equal to the control horizon ($N_p=N_c=3$) in this paper.

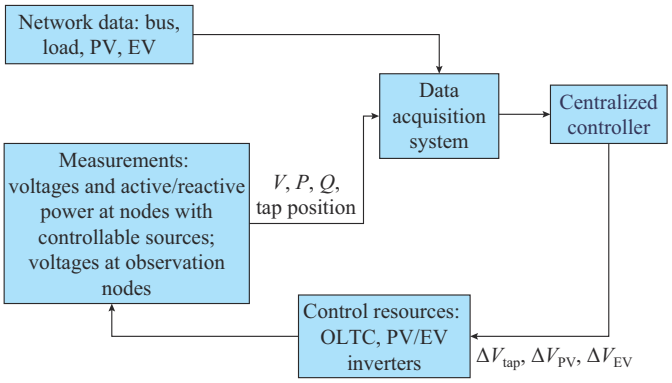

Fig. 2. Voltage control architecture in ADNs.

III. Optimization Problem Formulation

The optimal input change is found by an optimization problem which lies at the core of MPC. The objective function is formulated as a quadratic programming:

$$\min\left\{\sum_{l=1}^{N_p}\left(\left\|\boldsymbol{y}_{ref}-\boldsymbol{y}(k+l)\right\|_{\boldsymbol{Q}}^{2}+\left\|\boldsymbol{\sigma}\right\|_{\boldsymbol{S}}^{2}\right)+\left\|\Delta \boldsymbol{u}(k+l)\right\|_{\boldsymbol{R}}^{2}\right\} \tag{15}$$

where $\boldsymbol{y}_{ref}$ is the desired/reference vector; $\boldsymbol{\sigma}=[\sigma_1,\ \sigma_2]^{\mathrm{T}}$ is the slack variable vector added to the objective function so that the controller does not stop under solution infeasibility; and $\boldsymbol{Q}$, $\boldsymbol{R}$, and $\boldsymbol{S}$ are the weight matrices corresponding to the voltage deviation from the nominal value, control inputs, and slack variables, respectively. The objective function is convex and is solved as a standard quadratic problem with the positive semi-definite Hessian matrix. It is to be noted that the provided control strategy is deterministic in nature. The inherent uncertainties in nodal power may render the controller with insufficient control capability. Thus voltage constraints are relaxed using slack variables with the minimum possible value to secure the MPC controller from being stopped unintentionally. The weights are dynamically changed as per the requirement of the system. When the voltages are beyond the normal operation range, the weight associated with the control input change is reduced to bring the voltages quickly within the normal range and the weight associated with the voltage deviation from the nominal value is increased. Moreover, matrix $\boldsymbol{R}$ includes the weights corresponding to tap operation, active and reactive power control inputs of PVs and EVCSs, i.e., R_t, R_q, and R_p, respectively. The control inputs concerning active power are penalized more than reactive control inputs. The weights associated with control inputs under different network conditions are given in Table II. The values in Table II mean the objective weights of the weight matrices, i.e., the values of the diagonal elements. The optimal control action is obtained under the following system and input constraints:

$$\Delta \boldsymbol{u}_{\min}\le\Delta \boldsymbol{u}(k+l)\le\Delta \boldsymbol{u}_{\max} \tag{16}$$

$$\boldsymbol{u}_{\min}\le\boldsymbol{u}(k+l)\le\boldsymbol{u}_{\max} \tag{17}$$

$$-\sigma_1\boldsymbol{1}+\boldsymbol{v}_{\min}\le\boldsymbol{v}(k+l)\le\boldsymbol{v}_{\max}+\sigma_2\boldsymbol{1} \tag{18}$$

$$\boldsymbol{i}(k+1)\le\boldsymbol{i}_{\max} \tag{19}$$

TABLE II
WEIGHTS ASSOCIATED WITH CONTROL INPUTS UNDER DIFFERENT NETWORK CONDITIONS

Range of bus voltages (p.u.)	Objective weight				
	Q	R_t	R_q	R_p	S
$\max(\boldsymbol{v}) \geq 1.1$ or $\min(\boldsymbol{v}) \leq 0.9$	100	0.1	0.1	1	1000
$1.05 \leq \max(\boldsymbol{v}) \leq 1.1$ or $0.9 \leq \min(\boldsymbol{v}) \leq 0.95$	100	1	1	10	1000
$\max(\boldsymbol{v}) \leq 1.05$ and $\min(\boldsymbol{v}) \geq 0.95$	100	10	10	100	1000

$$\boldsymbol{v}(k+l)=\boldsymbol{v}(k+l-1)+\left[\frac{\delta \boldsymbol{v}}{\delta \boldsymbol{u}}\right]\Delta \boldsymbol{u}(k+l-1) \tag{20}$$

$$\boldsymbol{i}(k+l)=\boldsymbol{i}(k+l-1)+\left[\frac{\delta \boldsymbol{i}}{\delta \boldsymbol{u}}\right]\Delta \boldsymbol{u}(k+l-1) \tag{21}$$

where the subscripts min and max represent the minimum and maximum values of the corresponding variables, respectively; and **1** represents a unitary vector. Constraint (19) corresponds to the thermal limit constraints of the distribution lines. The MPC-based optimization is carried out in two stages. The optimal operation of OLTC is carried through each hour at the first stage, wherein $\Delta \boldsymbol{u}$ in (15) is given as:

$$\Delta \boldsymbol{u}=\Delta \boldsymbol{v}_{ref} \tag{22}$$

The variable $\Delta \boldsymbol{v}_{ref}$ (change in OLTC tap reference) is treated as a continuous variable. The appropriate action taken by the OLTC is determined by rounding off the value of the continuous variable obtained, to the nearest discrete tap position of the OLTC. At the second stage, controllable PV and EV inverters are coordinated after each minute, wherein the control input $\Delta \boldsymbol{u}$ in (15) is given by:

$$\Delta \boldsymbol{u}=[\Delta \boldsymbol{Q}_{pv}^{\mathrm{T}} \quad \Delta \boldsymbol{Q}_{ev}^{\mathrm{T}} \quad \Delta \boldsymbol{P}_{pv}^{\mathrm{T}} \quad \Delta \boldsymbol{P}_{ev}^{\mathrm{T}}]^{\mathrm{T}} \tag{23}$$

where $\Delta \boldsymbol{Q}_{pv}$ and $\Delta \boldsymbol{Q}_{ev}$ are the changes in reactive power exchanged by the PV inverters and EVCS inverters, respectively; and $\Delta \boldsymbol{P}_{pv}$ and $\Delta \boldsymbol{P}_{ev}$ are the changes in active power exchanged by the PV inverters and EVCS inverters, respectively. It is to be noted that the reactive power as well as active power from PV and EVCS is used as control variables. The active power from EVCS is considered to be available through EVCS smart inverters, to assess the control capability of V2G technology. The use of active power curtailment (APC) from PVs involves the curtailment of renewable energy, which is generally discouraged by the DG owners. Similarly, active power exchange by the EVCS involves the degradation of battery life and customer willingness to participate in V2G. Thus, a maximum of 10% of the available active power is used for control purposes. Moreover, the weights attributed to the control inputs associated with active power are considered significantly greater compared with those pertaining to reactive power control inputs, to exhibit the minimal preference for the active power. The dual-stage MPC efficiently deals with temporal characteristics of slow-acting OLTC and fast-acting PV and EV inverters, which greatly reduces unnecessary tap operation.

IV. REDUCED MODEL FRAMEWORK

The reduced model framework uses only selected nodes in MPC linear model formulation to reduce the model size for fast computation. This involves the identification of critical nodes and ranking of control resources as discussed in this section.

A. Selection of Observation Nodes

The multi-step corrective control using MPC needs real-time measurements to update the system state. For large-scale networks with substantial amounts of control resources, the need for measuring infrastructure increases significantly. The need for a wide communication network and measuring infrastructure throughout the network elevates the cost and complexity of real-time coordinated control. To achieve effective control with the requirement of least measurement infrastructure, we need to nominate network nodes that are more sensitive to deviations in network quantities such as voltage. For the identification of sensitive nodes, network partitioning using HCA [39] is used to dispense the network into the optimal number of zones. The HCA utilizes the concept of electrical distances defined in (24). The electrical distance D_{ij} quantifies the coupling among network nodes using voltage sensitivity [14].

$$D_{ij}=-\ln(\alpha_{ij}\alpha_{ji}) \tag{24}$$

where $\alpha_{ij}=\Delta V_i/\Delta V_j$ and $\alpha_{ji}=\Delta V_j/\Delta V_i$ are the voltage deviations at node i and node j with respect to voltage deviation at node j and node i, respectively.

1) HCA

The HCA initially assumes all nodes of the network as individual clusters. The clusters are subsequently merged using bottom-up agglomeration based on electrical distances, in a hierarchical manner as shown in Fig. 3.

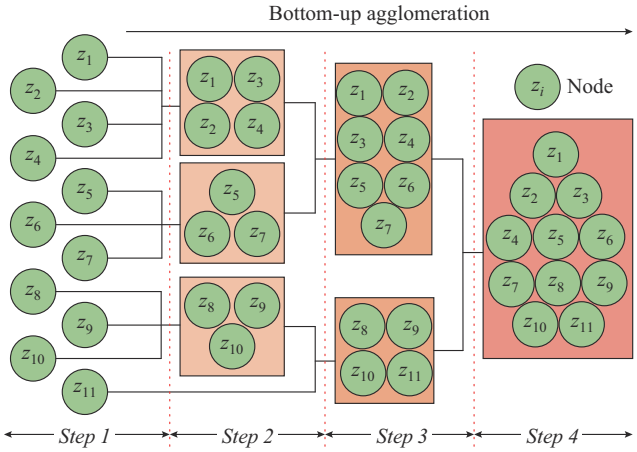

Fig. 3. Illustration of hierarchical clustering method.

The successive merging of individual clusters $\mathcal{C}_m$ and $\mathcal{C}_n$ is given by:

$$D_{mn}^{c}=\max\{D_{ij}: i\in\mathcal{C}_m, j\in\mathcal{C}_n\} \tag{25}$$

$$\mathcal{C}_m \cup \mathcal{C}_n=\min D_{mn}^{c} \tag{26}$$

where D_{mn}^{c} is the inter-cluster distance between cluster m and cluster n. The merging of zones of the network subsequently proceeds to form a single cluster. The appropriate clustering results are identified based on the measure of relative diame-

ter at each clustering stage. The diameter of a cluster d^c is given by:

$$d^c = \max\{D_{ij}: i,j \in \mathcal{C}\} \tag{27}$$

where $\mathcal{C}$ is the cluster for which diameter is calculated. If the number of zones at a given clustering stage is K, the relative diameter d^r of the network is given by:

$$d^r = \frac{1}{K}\sum_{i=1}^{K} d_i^c \tag{28}$$

The appropriate clusters K are chosen at the stage where the relative diameter change between successive stages is the maximum, i.e.,

$$K := \max\left\{\left|d_2^r - d_1^r\right|, \left|d_3^r - d_2^r\right|, ..., \left|d_{end}^r - d_{end-1}^r\right|\right\} \tag{29}$$

In var control space, the clusters are linked based on average linking criterion [39], wherein the inter-cluster distance is the average of electrical distances between the nodes of two clusters, given as:

$$D_{mn}^c = \frac{1}{\sum_{l=1}^{m_{\max}} n_m^l \sum_{l=1}^{n_{\max}} n_n^l} \sum_{i \in \mathcal{C}_m} \sum_{j \in \mathcal{C}_n} D_{ij} \tag{30}$$

where $n_m^l \in C_m$ and $n_n^l \in \mathcal{C}_n$ are the l^{th} nodes in clusters $\mathcal{C}_m$ and $\mathcal{C}_n$, respectively; and $m_{\max}$ and $n_{\max}$ are the total numbers of nodes in clusters $\mathcal{C}_m$ and $\mathcal{C}_n$, respectively. The appropriate clustering (with k clusters) is decided based on the maximum value of the average zone distance d^{av} of the network at each stage, given by:

$$d^{av} = \sqrt{\frac{\sum (cd_{mn})^2}{K}} \quad m,n = 1,2,...,k-1 \tag{31}$$

$$K := \max\{d_1^{av}, d_2^{av}, ..., d_{end}^{av}\} \tag{32}$$

where cd_{mn} is the inter-cluster distance between any two zones as calculated by (30) at a given clustering stage; and $d_1^{av}, d_2^{av}, ..., d_{end}^{av}$ are the average zone distances at different clustering stages. The optimal zoning corresponds to the value of K at the clustering stage where the value of zone distance is the maximum. Within each partition of the network, a node is chosen to represent the whole partition for any voltage variations. The representative nodes are named as observation nodes as in [43], which are chosen based on their location in the zone. For each zone, the PV node which lies towards the end of the feeder is chosen as the observation node [14]. However, if no PV node happens to be present in a zone, the node at the end of the feeder in the host zone is selected as the observation node. It is worth mentioning that for enhanced observability, we can choose multiple observation nodes from each zone so that the solution is closer to the system-wide optimal solution. However, due to the close geographical proximity of nodes in a zone in a distribution network, the generation profile of all PV-DG units is almost identical, thus it is sufficient to choose the single most critical observation node for the sensing and measurement of voltage control. Moreover, the slight change in sensitivity coefficients due to changes in network conditions has a negligible effect on electrical distances and no effect on the network partitioning. Thus, the partitioning remains the same in different load scenarios. It is to be noted that all observation nodes and nodes where controlled resources such as PVs or EVCSs are connected are necessarily equipped with measuring devices for real-time control. The communication infrastructure is laid only for nodes where control resources are connected.

B. Selection of the Minimum Control Resources

To minimize communication and the need of all voltage control resources, the control infrastructure is reduced by choosing the control nodes that are more significant in reducing the voltage violations with minimum control actions. For choosing the control resources for real-time control, the resources are ranked based on voltage sensitivities to the observation node. The ranking utilizes the numerical voltage sensitivity analysis carried out using offline power flow. Corresponding to each PV node, the value of the ranking index *RI* is calculated, which is the summation of voltage sensitivities at all observation nodes due to the reactive power change by a control resource. If $\mathcal{N}_{obsv} = \{o_1, o_2, ..., o_m\}$ is the set of observation nodes, and $\mathcal{N}_c = \{c_1, c_2, ..., c_n\}$ is the set of control resources available in the network, *RI* is given as:

$$RI_i = \frac{\partial v_{o_1}}{\partial Q_{c_i}} + \frac{\partial v_{o_2}}{\partial Q_{c_i}} + ... + \frac{\partial v_{o_r}}{\partial Q_{c_i}} + ... + \frac{\partial v_{o_m}}{\partial Q_{c_i}} \tag{33}$$

where RI_i is the index value corresponding to the i^{th} control resource; and $\partial v_{o_r}/\partial Q_{c_i}$ is the voltage sensitivity of the r^{th} observation node corresponding to reactive power change by the i^{th} control resource. The control resource with a higher value of *RI* is more effective in controlling the voltage at observation nodes. For the determination of the minimum set among all control resources (PV inverters), a simulation is performed to observe the highest voltage violation in the network. To correct the highest voltage violation, the control resources in the ranked set are sequentially added for voltage correction till the voltage violation is brought within the permissible limits [0.95, 1.05]p.u.. It is to be mentioned that the control resources are assumed to have the minimum reactive power available in this worst-case scenario. Thus, the control resource set that brings voltages within limits during the maximum violation is sufficient for controlling voltage violations throughout the network for all scenarios and load variations.

V. Modeling and Description of Test Distribution Networks

To validate the proposed control strategy, the test distribution network models are set up with the modified network configuration and added components. The network nodes are represented by set $\mathcal{N}$. The distribution lines radially connecting the nodes of the network are represented by a set $\mathcal{E} = (m,n) \subset \mathcal{N} \times \mathcal{N}$. The distribution system lines are modelled using series admittance, $y_{mn} = 1/(r_{mn} + jx_{mn})$, where r_{mn} and x_{mn} are the resistance and reactance of the line connecting nodes m and n, and $x_{mn} = \omega L_{mn}$, where L_{mn} and ω are the line inductance and system frequency, respectively. The 33-bus distribution network [13] and modified IEEE 123-bus distribution network [2] are used as test networks in this paper, as shown in Figs. 4 and 5, respectively.

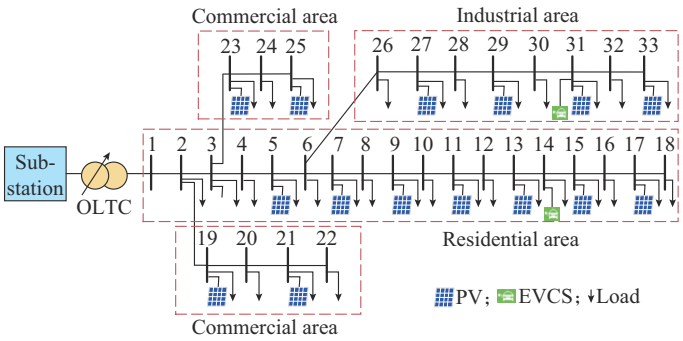

Fig. 4. 33-bus distribution network.

The peak active and reactive power demands of the 33-bus distribution network are 3.715 MW and 2.30 Mvar, respectively. The network is modified to accommodate 16 PVs of 550 kVA (each with peak generation of 500 kW) and two EVCSs of 1 MVA.

Similarly, the peak active and reactive power demand of the IEEE 123-bus distribution network is 3.49 MW and 1.92 Mvar, respectively. A total of 21 PV sources of 650 kVA are installed throughout the network with a peak generation of 585 kW. The PV inverters are slightly overrated by 10% to meet the reactive power demand as per IEEE standard 1547 (2018) [44].

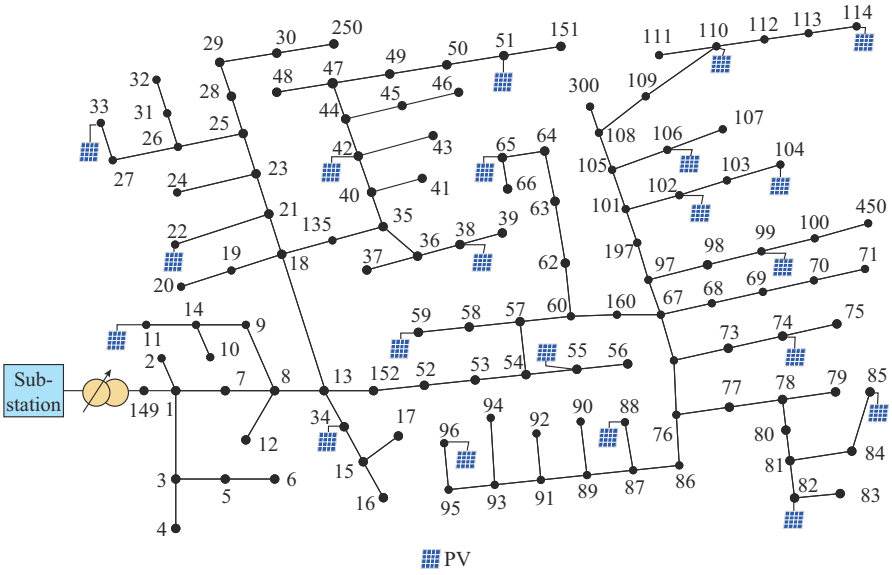

Fig. 5. Modified IEEE 123-bus distribution network.

It is to be noted that the distribution systems considered in this paper are assumed to be three-phase balanced systems. The substation is equipped with an OLTC, which is coordinated in a centralized control strategy for regulating the distribution system voltage. The tap operation of OLTC for voltage control, as in [45], is given by:

$$\dot{\chi}=-H\chi+K(v_t-v_{ref}) \tag{34}$$

where v_t is the voltage at the secondary side of the OLTC; v_{ref} is the reference voltage of OLTC, which is the control variable as defined in (22); and χ, H, and K are the state variable (tap position), integral deviation, and inverse time constant, respectively, and the variable χ corresponding to the tap operation is treated as a continuous variable. However, the value of χ depends on v_{ref}, which is determined by the optimization at the first stage. The OLTC has 32 tap steps and one tap step changes the voltage by 0.00625 p.u., and a maximum of 2 tap steps are allowed at a given time instant. Thus, OLTC can step up or bring down the voltage by 0.1 p. u. when the highest or lowest tap positions are reached. The parameters K and H are toned so that the OLTC control action is completed in 3 s. It is to be mentioned that the tap operation is carried only when then the maximum voltage deviation in the network is more than 2.5% of the nominal value, and the total number of tap operations in a day is restricted to be 10 to enhance its life. Furthermore, PV sources are connected to the balanced three-phase distribution network at various nodes, which are assumed to be interfaced by smart inverters, so that they can exchange active as well as reactive power with the network. The nodes where PV sources are connected are represented by node set $\mathcal{N}_{PV}\subset\mathcal{N}$. The PV power generation relies on PV capacity and irradiance at a given location and time. The available reactive power of PVs and EV stations, i.e., $Q_{PV}(t)$ and $Q_{EV}(t)$, are constrained by active power generation and EV charging load as given in (35) and (36), respectively. The inverters are assumed to have grid support functions to exchange reactive power under very little or no active power generation.

$$Q_{PV}(t)=\pm\sqrt{S_{PV}^2-P_{PV}^2(t)} \tag{35}$$

$$Q_{EV}(t)=\pm\sqrt{S_{EV}^2-P_{EV}^2(t)} \tag{36}$$

where $P_{PV}(t)$ and $P_{EV}(t)$ are the active power exchanged at time instant t by a PV source and an EVCS, respectively; and S_{PV} and S_{EV} are the ratings of the PV inverter and EVCS inverter, respectively. The power profile of PVs can significantly vary with geographic location. Since distribution networks are located in a small geographical area, the generation profile is assumed to be uniform for all PVs in both the 33-bus and the modified IEEE 123-bus distribution net-

works. The PV generation profile and EV load profile are shown in Fig. 6(a). The loads are connected in all nodes. These are classified as residential loads, industrial loads, and commercial loads Fig. 6(b), and the load power demand is shown.

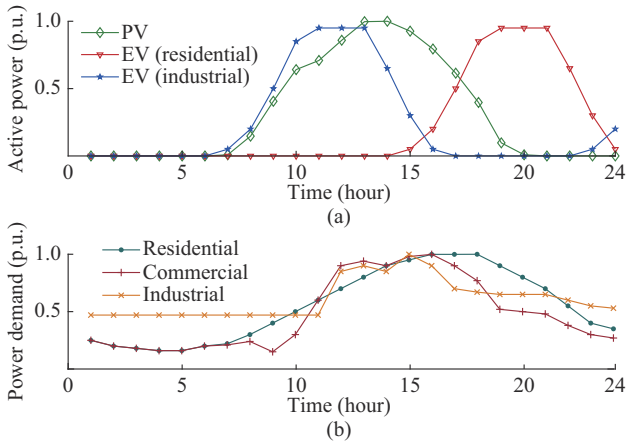

Fig. 6. Power profiles. (a) PV generation and EV load. (b) Load power demand.

VI. Simulation Results and Discussion

The proposed control strategy is validated on the 33-bus distribution network and modified IEEE 123-bus distribution network. The networks are modeled using the Power System Analysis Toolbox (PSAT) in MATLAB environment and all optimizations are carried out using CPLEX solver with MATLAB interface.

A. 33-bus Distribution Network

Simulations are performed on the 33-bus distribution network shown in Fig. 4. The network is fed from 63.3 kV/12.66 kV substation at node 1. The system base power is considered as 10 MVA and the base voltage is 12.66 kV. The PV sources are distributed throughout the network with two EVCSs located at node 14 and node 31 as in [13], one OLTC at the substation, and industrial, commercial, and residential loads (Fig. 4). Initially, the distribution network is partitioned into 4 zones using HCA to identify the observation nodes, as depicted in Fig. 7.

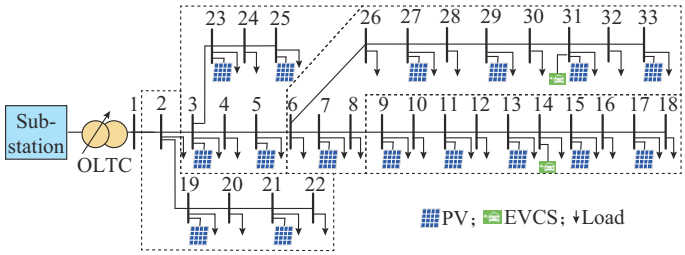

Fig. 7. Partitioning of 33-bus distribution network.

The network nodes $\mathcal{N}_{obsv} \subset \mathcal{N} = \{17, 33, 5, 21\}$ are chosen as observation nodes based on their location at the feeder end in a zone [14]. Corresponding to these observational nodes, all PV control sources are ranked based on the value of *RI*. The ranking of PV inverters for voltage control is shown in Table III.

To effectively choose an optimal set of controllable PV resources $\mathcal{N}_{cont} \subset \mathcal{N}_{PV}$, a time domain simulation over 24 hours is run to determine the instant of extreme voltage violations in the network. The simulation is carried out assuming there is no voltage control available in the network. The voltage profile without any control action is shown in Fig. 8, where the gray planes represent the upper and lower limits of normal operation range of node voltages, which are 1.05 p.u. and 0.95 p.u., respectively.

TABLE III
Ranking of PV Inverters for Voltage Control in 33-bus Distribution Network

Ranking	PV bus	*RI*	Ranking	PV bus	*RI*
1	33	0.5047	9	7	0.2291
2	17	0.4878	10	27	0.2246
3	31	0.4429	11	21	0.1365
4	15	0.4008	12	5	0.1229
5	13	0.3527	13	25	0.0563
6	29	0.3526	14	23	0.0553
7	11	0.3022	15	3	0.0549
8	9	0.2695	16	19	0.0208

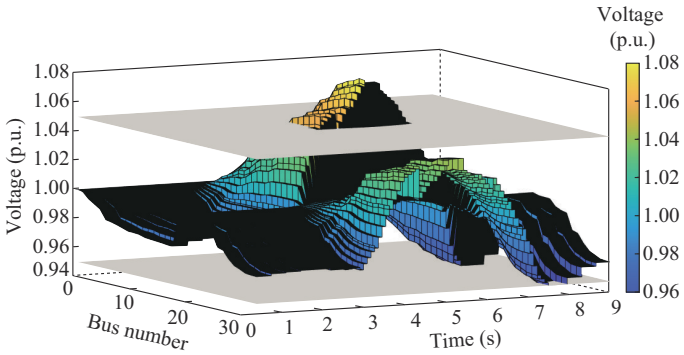

Fig. 8. Voltage profile without any control action in 33-bus distribution network.

The extreme voltages are 1.0826 p.u. and 0.9429 p.u. at node 17 and node 18, respectively. Since the peak over-voltage violation is greater than the peak under-voltage violation, the over-voltage scenario under the given network conditions and available reactive power from PV inverters are considered for voltage correction. The control resources from the ranked set are serially added for extreme voltage correction, to bring down the node voltage below the normal operation limit (1.05 p.u.). The voltage correction for extreme over-voltage scenario requires the top five ranked PV sources $\mathcal{N}_{cont} = \{33, 17, 31, 15, 13\}$ for bringing the voltage within limits. The voltage control for the test network is studied considering two cases as follows.

1) Case A: only PVs and coordinated control of PVs and OLTC are used for voltage control assuming that no EV load is present in the distribution network.

2) Case B: EV loads are added to the 33-bus distribution network at node 14 and node 31 and are centrally coordinated with PVs and OLTC for voltage control.

The voltage profiles and test results are given in Figs. 9-

13, and will be discussed in the following text.

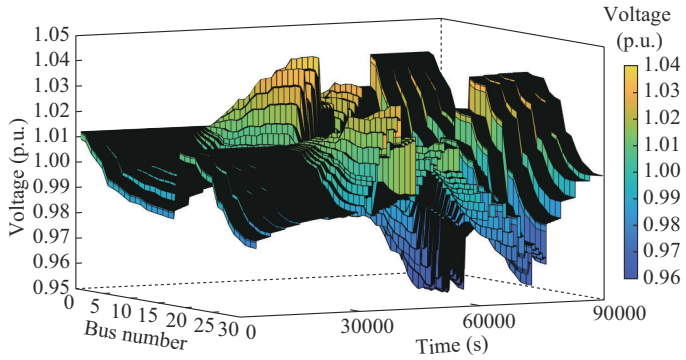

Fig. 9. Voltage profile with coordinated control of PV inverters and OLTC in 33-bus distribution network.

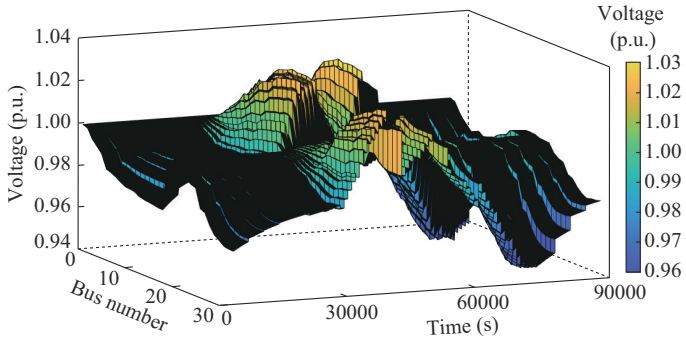

Fig. 10. Voltage profile with coordinated control of PV inverters in 33-bus distribution network.

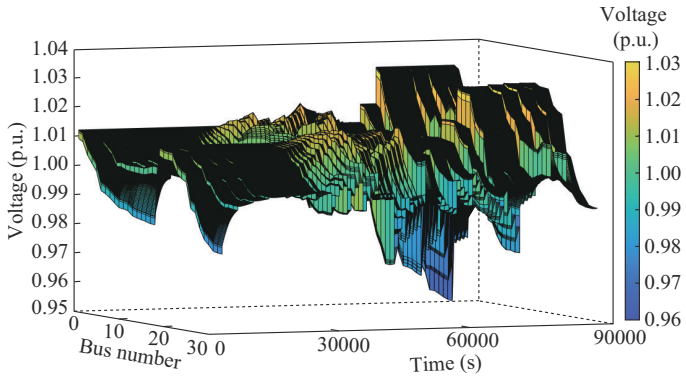

Fig. 11. Voltage profile with coordinated control of OLTC, PV inverters, and EVCSs in 33-bus distribution network.

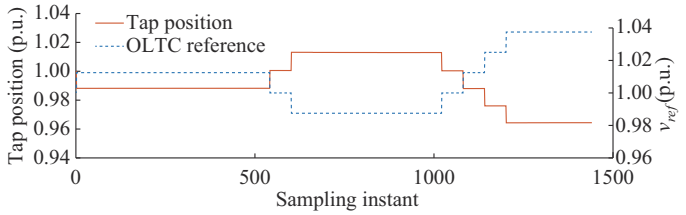

Fig. 12. OLTC tap operation with coordinated control of PV inverters and OLTC in 33-bus distribution network.

1) Case A

The network is modelled for observation nodes and node-set $\mathcal{N}_{cont}$. It is considered that the measuring devices are placed at all modeled nodes and the substation, while communication infrastructure is laid for node set $\mathcal{N}_{cont}$ and the substation node.

The PV inverters of set $\mathcal{N}_{cont}$ are used to eliminate voltage violations corresponding to the PV generation profile in Fig. 6(a) and load profile in Fig. 6(b) using single-stage MPC, assuming no OLTC control. The voltage profile with coordinated control of PV inverters is shown in Fig. 10.

It can be seen that the voltages remain within the safe operation limits [0.95,1.05]p.u.. It is to be noted that only selected control resources are sufficiently able to maintain voltages within the limits. The reactive power exchange by these resources is high from the available reactive power inverter. Furthermore, the controller tries to bring the voltages closer to the nominal value when the voltages are within limits so that the power losses are reduced; however, we can relax this objective to reduce reactive power exchange for any economical or operational constraints of the inverters. The highest and lowest voltages of PV inverters without APC are 1.0460 p.u. and 0.9503 p.u., respectively. Under added control using APC, the minimum/maximum voltage is 1.0349/0.9510 p.u., and the total curtailed active power is 8.5 kWh, as shown in Fig. 13(a).

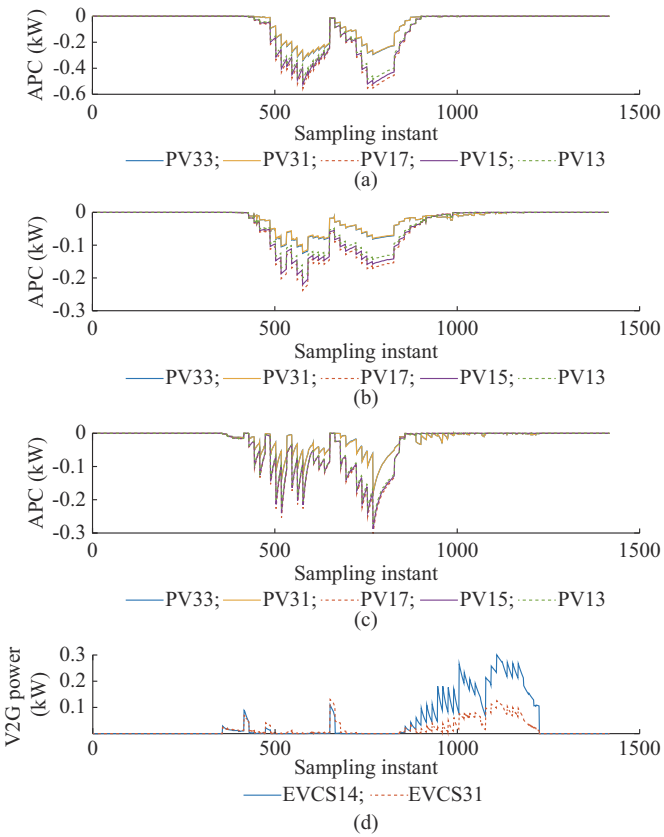

Fig. 13. Active power exchange by control resources. (a) APC in Case A with only PV control. (b) APC in Case A with coordinated control of OLTC and PV inverters. (c) APC in Case B with coordinated control of PV inverters, EVCS, and OLTC. (d) Active power injection from EVCS using V2G in Case B.

Figure 9 shows the voltage profile with coordinated control of PV inverters and OLTC using the dual-stage MPC framework. The OLTC tap operation is carried out using if-

then-else rules in addition to being centrally coordinated with the controlled PV inverters. The OLTC operation is optimally determined after each hour, and 6 tap operations are dispatched by the central controller (Fig. 12). The OLTC takes 3 s to apply each tap control action. It is to be understood that the OLTC operates with primary winding control, thus increasing the tap position reduces the secondary voltage. Since the reference voltage corresponds to the secondary voltage, the reference voltage above 1 p.u. results in a decrease in tap position and vice versa. The primary voltage is always 1 p.u., with each tap step at the secondary voltage changes by 0.00625 p.u.. Since the voltages are maintained within limits by PV inverters only, the coordination of OLTC tries to bring voltages closer to the nominal value and reduces the net reactive power injection and absorption significantly. The tap operation can be further reduced by relaxing the objectives of voltage deviations from the nominal value. However, we may have other objectives such as power loss minimization in the optimization formulation. The maximum and minimum voltages after the coordinated control of PV inverters and OLTC are 1.0454 p.u. and 0.9504 p.u., respectively, and the net curtailed power is 3.6 kW, as shown in Fig. 13(b). The APC reduces the reactive power injection and absorption requirements by 0.6411 MVA and 1.5983 MVA, respectively, as compared with the control without leveraging APC.

2) Case B

An EV load is added to the network in the residential and industrial sections. The EVCSs are placed at node 14 and node 31 of the network, each rated 1 MVA. The EV load profile is shown in Fig. 6(a). Simulations are carried out to observe the effects of adding EV load. The EV inverters are brought in for actively controlling voltages with active power as well as reactive power exchange in coordination with OLTC and PV inverters, to show their effectiveness in voltage regulation and V2G capabilities. The EV inverters are coordinated with OLTC and PV inverters, assuming that they are equipped with measuring devices and communication to other control devices and the centralized controller (at the substation). The voltage profile with coordinated control of OLTC, PV inverters, and EVCSs is shown in Fig. 11, with the minimum and maximum voltages as 1.0312 p.u. and 0.9554 p.u., respectively. By leveraging reactive power from PV inverters, the minimum voltage is brought up from 0.9700 p.u. to 0.9742 p.u.. The net APC and active power injection from EVCS are 3.1 kW and 1.4 kW, respectively, as shown in Fig. 13(c) and Fig. 13(d), respectively. Even though the active power exchange is less, it significantly reduces the need for reactive power exchange.

To validate the efficacy of the proposed strategy with reduced measuring infrastructure and control resources compared with the full-order models, a comparison is made with single-stage MPC in [14] and dual-stage MPC in [13]. Bus 17 is chosen for analysis due to its highest voltage violation and the voltage profiles are shown in Fig. 14.

Various metrics such as the minimum and maximum voltages, reactive power injection and absorption, and total network power losses are used for comparison, as given in Table IV.

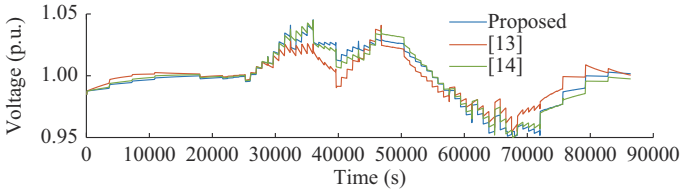

Fig. 14. Comparison of voltage profiles of bus 17 using reduced model framework with full-order models.

TABLE IV
COMPARISON OF CONTROL STRATEGIES

Control strategy	Test distribution network	The minimum/maximum voltage (p.u.)	Reactive power injection/absorption (MVA)	Power loss (MWh)
[13]	33-bus	0.9520/1.0425	2.8859/8.7592	2.8295
	Modified IEEE 123-bus	0.9786/1.0250	9.9426/7.2572	5.5326
[14]	33-bus	0.9511/1.0454	2.9802/8.3960	2.8166
	Modified IEEE 123-bus	0.9760/1.0250	8.0654/6.9671	5.5618
Proposed	33-bus	0.9521/1.0476	2.1937/8.2233	2.7488
	Modified IEEE 123-bus	0.9757/1.0204	6.1761/6.8278	5.7884

It is seen that the reduced model framework performs efficiently with all the metrics quite comparable to the full-order models [13]. Furthermore, a numerical comparison is provided in Table V to quantify the voltage deviation in both models. In the table, μ is the mean voltage difference, and σ is the standard deviation of the voltage difference between the full-order model and the reduced-order model, over the whole simulation period of 24 hours. Both mean and standard deviations are quite low, which infers that the reduced model framework performs similarly to the full-order model.

TABLE V
COMPARISON BETWEEN FULL-ORDER MODEL AND REDUCED-ORDER MODEL

Test distribution network	System model	Number of nodes modelled	Optimization running time per sample (s)	Voltage deviation (p.u.)	
				μ	σ
33-bus	Full-order model	33	0.0312	0.0067 (node 17)	0.0085
	Reduced-order model	8	0.0186		
Modified IEEE 123-bus	Full-order model	123	0.0505	0.0034 (node 94)	0.0043
	Reduced-order model	7	0.0183		

Considering the communication latency of 150 ms for transferring the set of measurements to the central controller, the complete execution of the control action by the inverters requires 0.3186 s using the proposed strategy. Nevertheless, the time step for the MPC control is chosen as 1 min. The MPC control can be efficiently used for small time steps if the fast variation in generation and load are considered.

B. Modified IEEE 123-bus Distribution Network

The proposed strategy is further validated on a larger modified IEEE 123-bus distribution network. The modified network is a balanced three-phase network with a nominal voltage of 4.16 kV. The system base power and base voltage are chosen to be 1 MVA and 4.16 kV, respectively. The network is fed through an OLTC at node 149 and PVs are distributed as shown in Fig. 5 with ratings described in Section VI. The network is partitioned into 6 zones using HCA, as shown in Fig. 15, and the identified set of observation nodes is $\mathcal{N}_{obsv} \subset \mathcal{N} = \{114, 85, 59, 51, 11, 6\}$. Corresponding to the observation nodes, the PVs are ranked as shown in Table VI.

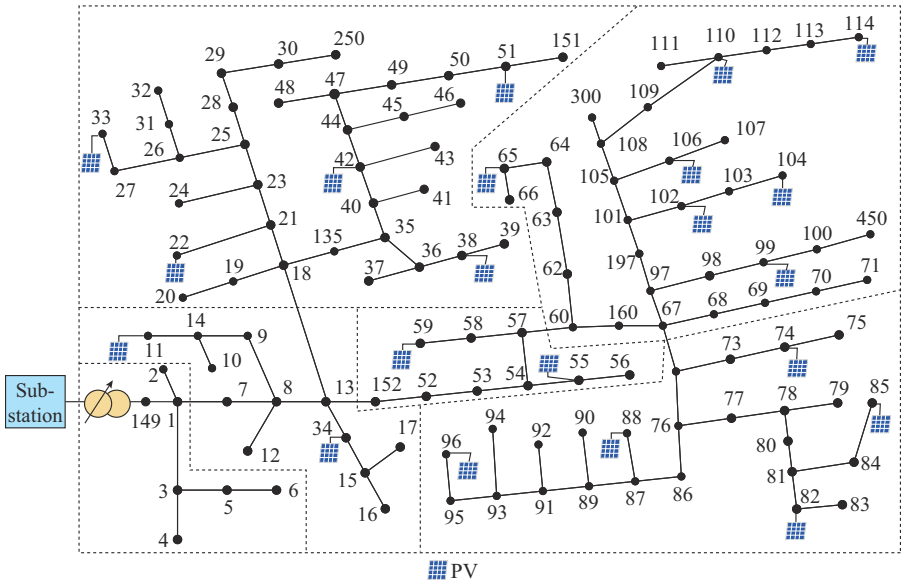

Fig. 15. Partitioning of modified IEEE 123-bus distribution network using HCA.

TABLE VI
RANKING OF CONTROL RESOURCES IN MODIFIED IEEE 123-BUS DISTRIBUTION NETWORK

Ranking	PV bus	*RI*	Ranking	PV bus	*RI*	Ranking	PV bus	*RI*
1	85	0.2161	8	104	0.1763	15	55	0.1187
2	114	0.2133	9	102	0.1760	16	42	0.1113
3	110	0.1969	10	74	0.1736	17	38	0.1043
4	82	0.1967	11	99	0.1726	18	33	0.0993
5	106	0.1798	12	65	0.1592	19	22	0.0990
6	96	0.1778	13	59	0.1422	20	34	0.0893
7	88	0.1774	14	51	0.1273	21	11	0.0659

The voltage profile without any control action is shown in Fig. 16, and the minimum and maximum voltages are 0.9272 p.u. and 1.0592 p.u., respectively. The minimum control resource set $\mathcal{N}_{cont} = \{85, 114, 110\}$ is seen to be sufficient to eliminate the extreme voltage violation in the network. The voltage profile using control resource set $\mathcal{N}_{cont}$ (PV inverters only) with single-stage MPC is shown in Fig. 17.

The minimum and the maximum voltages after coordinated control of PV inverters are seen to be 0.9673 p.u. and 1.0135 p.u., respectively, with a net APC of 2.3545 kW. The voltage profile using coordinated control of PV inverters and OLTC with dual-stage MPC is shown in Fig. 18.

The maximum and minimum voltages are seen to be 1.0187 p.u. and 0.9756 p.u., respectively, with 7 tap operations as shown in Fig. 19, thus maintaining the voltages with normal operation limits. Figure 20 shows the APC. The total APC from PVs is 2.0228 kW. The coordinated control of PV inverters and OLTC reduces the reactive power injection from 7.0257 MVA to 4.6071 MVA.

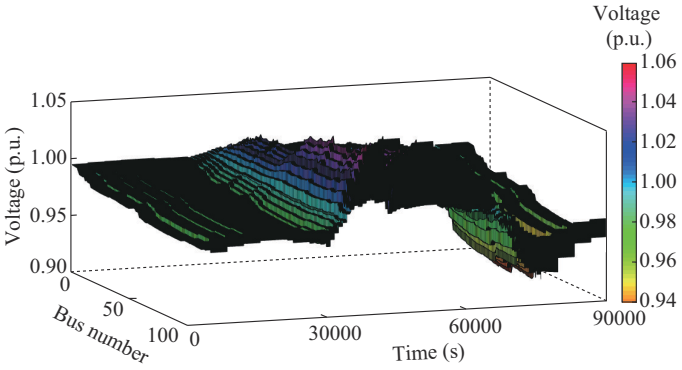

Fig. 16. Voltage profile without any control action in modified IEEE 123-bus distribution network.

A comparison of the full-order models proposed in [13] and [14] with the reduced-order model is provided in Fig. 21 with numerical comparison in Table VI.

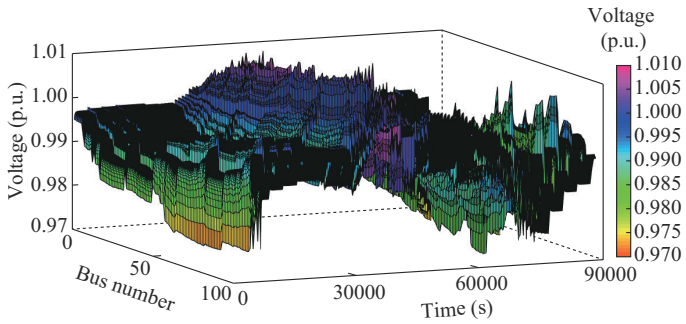

Fig. 17. Voltage profile using coordinated control of PV inverters in modified IEEE 123-bus distribution network.

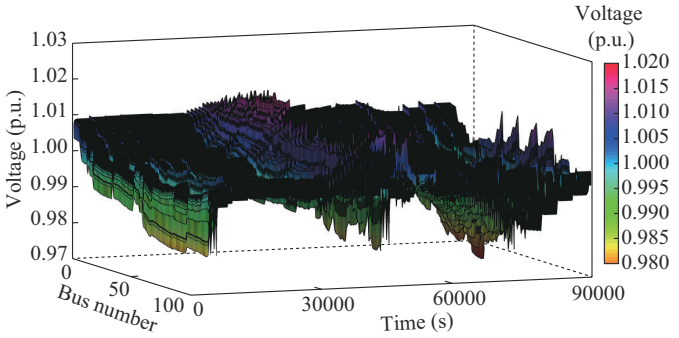

Fig. 18. Voltage profile with coordinated control of PV inverters and OLTC in modified IEEE 123-bus distribution network.

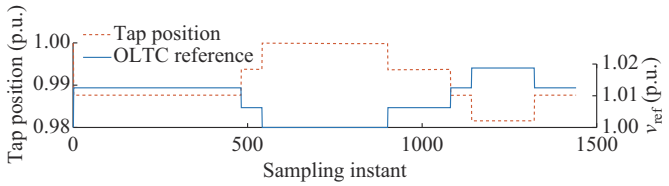

Fig. 19. OLTC tap operation with coordinated control of PV inverters and OLTC in modified IEEE 123-bus distribution network.

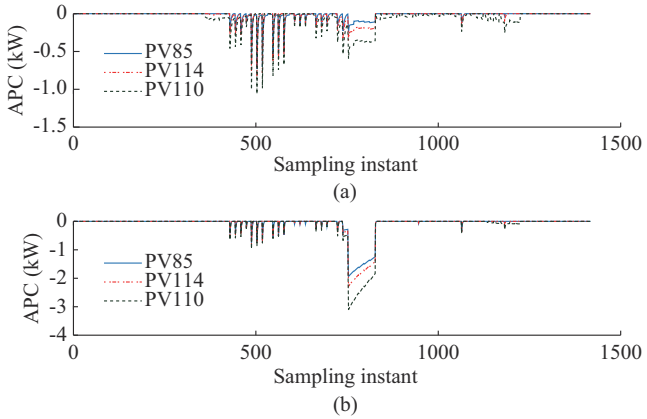

Fig. 20. APC. (a) Coordinated control of PV inverters. (b) Coordinated control of PV inverters and OLTC.

VII. Conclusion

In this paper, a voltage control strategy based on dual-stage model predictive control is presented using a reduced model framework, which utilizes a minimal set of available control resources to mitigate the need for system-wide communication, measuring infrastructure, and computation time.

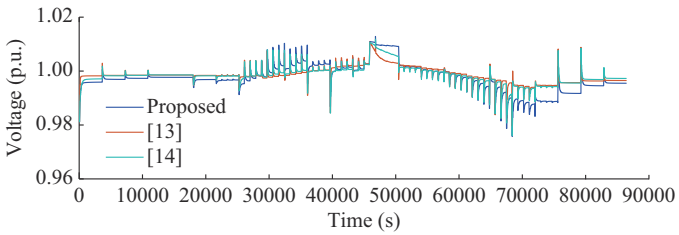

Fig. 21. Comparison of voltage profile of bus 94.

Unlike the full-order model, the observation and control nodes are only modeled using linear model for the MPC framework. Furthermore, the controllable nodes and critical observation nodes are assumed to have the necessary measuring infrastructure for real-time control. The minimal set of control resources is identified by ranking the system nodes with control resources, corresponding to critical observation nodes, using numerical voltage sensitivity analysis based novel index called ranking index. The efficacy of the proposed control strategy is verified on 33-bus and modified IEEE 123-bus distribution networks. The proposed control strategy efficiently performs in voltage regulation as compared with the full-order models.

References

[1] G. C. Kryonidis, E. O. Kontis, A. I. Chrysochos *et al.*, "A coordinated droop control strategy for overvoltage mitigation in active distribution networks," *IEEE Transactions on Smart Grid*, vol. 9, no. 5, pp. 5260-5270, Sept. 2018.

[2] Y. Chai, L. Guo, C. Wang *et al.*, "Network partition and voltage coordination control for distribution networks with high penetration of distributed PV units," *IEEE Transactions on Power Systems*, vol. 33, no. 3, pp. 3396-3407, May 2018.

[3] P. Li, H. Ji, C. Wang *et al.*, "Coordinated control method of voltage and reactive power for active distribution networks based on soft open point," *IEEE Transactions on Sustainable Energy*, vol. 8, no. 4, pp. 1430-1442, Oct. 2017.

[4] H. S. Bidgoli and T. V. Cutsem, "Combined local and centralized voltage control in active distribution networks," *IEEE Transactions on Power Systems*, vol. 33, no. 2, pp. 1374-1384, Mar. 2018.

[5] S. Singh, V. B. Pamshetti, and S. P. Singh, "Time horizon-based model predictive volt/var optimization for smart grid enabled CVR in the presence of electric vehicle charging loads," *IEEE Transactions on Industrial Applications*, vol. 55, no. 6, pp. 5502-5513, Dec. 2018.

[6] S. Martinenas, K. Knezovic, and M. Marinelli, "Management of power quality issues in low voltage networks using electric vehicles: experimental validation," *IEEE Transactions on Power Delivery*, vol. 32, no. 2, pp. 971-979, Apr. 2017.

[7] F. R. Islam, A. Lallu, K. A. Mamun *et al.*,, "Power quality improvement of distribution network using BESS and capacitor bank," *Journal of Modern Power Systems and Clean Energy*, vol. 9, no. 3, pp. 625-632, May 2021.

[8] R. B. Navesi, D. Nazarpour, R. Ghanizadeh *et al.*, "Switchable capacitor bank coordination and dynamic network reconfiguration for improving operation of distribution network integrated with renewable energy resources," *Journal of Modern Power Systems and Clean Energy*, vol. 10, no. 3, pp. 637-646, May 2022.

[9] A. Kulmala, A. Mutanen, A. Koto *et al.*, "RTDS verification of a coordinated voltage control implementation for distribution networks with distributed generation," in *Proceedings of 2010 IEEE PES Innovative Smart Grid Technologies Conference Europe (ISGT Europe)*, Gothenburg, Sweden, Oct. 2010, pp. 1-8.

[10] G. Valverde and T. van Cutsem, "Model predictive control of voltages in active distribution networks," *IEEE Transactions on Smart Grid*, vol. 4, no. 4, pp. 2152-2161, Dec. 2013.

[11] H. M. Nguyen, J. L. R. Torres, A. Lekic *et al.*, "MPC based centralized voltage and reactive power control for active distribution networks," *IEEE Transactions on Energy Conversion*, vol. 36, no. 2, pp.

1537-1547, Jun. 2021.
[12] A. Dutta, S. Ganguly, and C. Kumar, "Model predictive control-based optimal voltage regulation of active distribution networks with OLTC and reactive power capability of PV inverters," *IET Generation, Transmission & Distribution*, vol. 14, no. 22, pp. 5183-5192, Nov. 2020.
[13] A. Dutta, S. Ganguly, and C. Kumar, "Coordinated volt/var control of PV and EV interfaced active distribution networks based on dual-stage model predictive control," *IEEE Systems Journal*, vol. 16, no. 3, pp. 4291-4300, Sept. 2022.
[14] Y. Guo, Q. Wu, H. Gao *et al.*, "MPC-based coordinated voltage regulation for distribution networks with distributed generation and energy storage system," *IEEE Transactions on Sustainable Energy*, vol. 10, no. 4, pp. 1731-1739, Oct. 2019.
[15] A. Dutta, S. Ganguly, and C. Kumar, "MPC-based coordinated voltage control in active distribution networks incorporating CVR and DR," *IEEE Transactions on Industrial Applications*, vol. 58, no. 4, pp. 4309-4318, Aug. 2022.
[16] M. H. Hemmatpour, M. H. R. Koochi, P. Dehghanian *et al.*, "Voltage and energy control in distribution systems in the presence of flexible loads considering coordinated charging of electric vehicles," *Energy*, vol. 239-A, p. 121880, Jan. 2022.
[17] S. Maharjan, A. M. Khambadkone, and J. C. H. Peng, "Robust constrained model predictive voltage control in active distribution networks," *IEEE Transactions on Sustainable Energy*, vol. 12, no. 1, pp. 400-411, Jan. 2021.
[18] K. Christakou, M. Paolone, and A. Abur, "Voltage control in active distribution networks under uncertainty in the system model: a robust optimization approach," *IEEE Transactions on Smart Grid*, vol. 9, no. 6, pp. 5631-5642, Nov. 2018.
[19] L. Youbo, H. Gao, J. Y. Liu *et al.*, "Multi-agent based hierarchical power scheduling strategy for active distribution network," in *Proceedings of 2015 International Symposium on Smart Electric Distribution Systems and Technologies (EDST)*, Vienna, Austria, Sept. 2015, pp. 151-158.
[20] D. Hu, Z. Ye, Y. Gao *et al.*, "Multi-agent deep reinforcement learning for voltage control with coordinated active and reactive power optimization," *IEEE Transactions on Smart Grid*, vol. 13, no. 6, pp. 4873-4886, Nov. 2022.
[21] X. Dou. P. Xu, Q. Hu *et al.*, "A distributed voltage control strategy for multi-microgrid active distribution networks considering economy and response speed," *IEEE Access*, vol. 6, pp. 31259-31268, May 2018.
[22] J. Hu, C. Ye, Y. Ding *et al.*, "A distributed MPC to exploit reactive power V2G for real-time voltage regulation in distribution networks," *IEEE Transactions on Smart Grid*, vol. 13, no. 1, pp. 576-588, Jan. 2022.
[23] L. Yu, D. Czarkowski, and F. de Leon, "Optimal distributed voltage regulation for secondary networks with DGs," *IEEE Transactions on Smart Grid*, vol. 3, no. 2, pp. 959-967, Jun. 2012.
[24] L. Wang, R. Yan, F. Bai *et al.*, "A distributed inter-phase coordination algorithm for voltage control with unbalanced PV integration in LV systems," *IEEE Transactions on Sustainable Energy*, vol. 11, no. 4, pp. 2687-2697, Oct. 2020.
[25] M. Zeraati, M. E. H. Golshan, and J. M. Guerrero, "A consensus-based cooperative control of PEV battery and PV active power curtailment for voltage regulation in distribution networks," *IEEE Transactions on Smart Grid*, vol. 10, no. 1, pp. 670-680, Jan. 2019.
[26] A. N. M. M. Haque, M. Xiong, and P. H. Nguyen, "Consensus algorithm for fair power curtailment of PV systems in LV networks," in *Proceedings of 2019 IEEE PES GTD Grand International Conference and Exposition Asia (GTD Asia)*, Bangkok, Thailand, Mar. 2019, pp. 813-818.
[27] R. Hu, W. Wang, X. Wu *et al*., "Coordinated active and reactive power control for distribution networks with high penetrations of photovoltaic systems," *Solar Energy*, vol. 231, pp. 809-827, Jan. 2022.
[28] R. Haider and A. M. Annaswamy, "A hybrid architecture for volt-var control in active distribution grids," *Applied Energy*, vol. 312, p. 118735, Apr. 2022.
[29] H. J. Liu, W. Shi, and H. Zhu, "Hybrid voltage control in distribution networks under limited communication rates," *IEEE Transactions on Smart Grid*, vol. 10, no. 3, pp. 2416-2427, May 2019.
[30] F. Kabir, N. Yu, Y. Gao *et al.*, "Deep reinforcement learning-based twotimescale volt-var control with degradation-aware smart inverters in power distribution systems," *Applied Energy*, vol. 335, p. 120629, Apr. 2023.
[31] P. Li, M. Wei, H. Ji *et al*., "Deep reinforcement learning-based adaptive voltage control of active distribution networks with multi-terminal soft open point," *International Journal of Electrical Power & Energy Systems*, vol. 141, p. 108138, Oct. 2022.
[32] Q. Yang, G. Wang, A. Sadeghi *et al.*, "Two-timescale voltage control in distribution grids using deep reinforcement learning," *IEEE Transactions on Smart Grid*, vol. 11, no. 3, pp. 2313-2323, May 2020.
[33] P. Li, J. Ji, H. Ji *et al.*, "MPC-based local voltage control strategy of dgs in active distribution networks," *IEEE Transactions on Sustainable Energy*, vol. 11, no. 4, pp. 2911-2921, Oct. 2020.
[34] L. Wang, A. Dubey, A. H. Gebremedhin *et al.*, "MPC-based decentralized voltage control in power distribution systems with EV and PV coordination," *IEEE Transactions on Smart Grid*, vol. 13, no. 4, pp. 2908-2919, Jul. 2022.
[35] G. Lou, W. Gu, Y. Xu *et al.*, "Distributed MPC-based secondary voltage control scheme for autonomous droop-controlled microgrids," *IEEE Transactions on Sustainable Energy*, vol. 8, no. 2, pp. 792-804, April 2017.
[36] R. R. Hossain and R. Kumar, "A distributed-MPC framework for voltage control under discrete time-wise variable generation/load," *IEEE Transactions on Power Systems*, vol. 39, no. 1, pp. 809-820, Jan. 2024.
[37] W. Jiao, J. Chen, Q. Wu *et al.*, "Distributed coordinated voltage control for distribution networks with DG and OLTC based on MPC and gradient projection," *IEEE Transactions on Power Systems*, vol. 37, no. 1, pp. 680-690, Jan. 2022.
[38] K. Alzaareer, M. Saad, H. Mehrjerdi *et al.*, "Development of new identification method for global group of controls for online coordinated voltage control in active distribution networks," *IEEE Transactions on Smart Grid*, vol. 11, no. 5, pp. 3921-3931, Sept. 2020.
[39] V. Alimisis and P. C. Taylor, "Zoning evaluation for improved coordinated automatic voltage control," *IEEE Transactions on Power Systems*, vol. 30, no. 5, pp. 2736-2746, Sept. 2015.
[40] S. Nowak, Y. Chen, and L. Wang, "Distributed measurement-based optimal DER dispatch with estimated sensitivity models," *IEEE Transactions on Smart Grid*, vol. 13, no. 3, pp. 2197-2208, May 2022.
[41] S. Nowak, Y. Chen, and L. Wang, "Measurement-based optimal DER dispatch with a recursively estimated sensitivity model," *IEEE Transactions on Power Systems*, vol. 35, no. 6, pp. 4792-4802, Nov. 2020.
[42] L. Wang, "Discrete-time MPC with constraints," in *Model Predictive Control System Design and Implementation Using MATLAB*, 1st ed., London: Springer, 2009, pp. 43-78.
[43] S. Munikoti, M. Abujubbeh, K. Jhala *et al.*, "An information theoretic approach to identify dominant voltage influencers for unbalanced distribution systems," *IEEE Transactions on Power Systems*, vol. 37, no. 6, pp. 4436-4446, Nov. 2022.
[44] *IEEE Standard for Interconnection and Interoperability of Distributed Energy Resources with Associated Electric Power Systems Interfaces*, IEEE Std 1547-2018 (Revision of IEEE Std 1547-2003), Apr. 2018.
[45] F. Milano. (2011, Jun.). Power system analysis toolbox: documentation for PSAT version 2.1.6. [Online]. Available: https://www.eecs.wsu.edu/~ee521/Material/20120927/psat-20080214.pdf

Mudaser Rahman Dar received the B.Tech. degree in electrical engineering from Islamic University of Science & Technology, Kashmir, India, in 2017, and the M.Tech. degree in electrical power and energy systems from National Institute of Technology, Srinagar, India, in 2020. He is currently pursuing the Ph.D. degree in the Department of Electronics and Electrical Engineering, Indian Institute of Technology (IIT), Guwahati, India. His research interests include distribution system optimization, voltage control and stability in active distribution networks, and electric vehicle (EV) integration in power distribution networks.

Sanjib Ganguly received the B.Eng. degree in electrical engineering from Indian Institute of Engineering, Science, and Technology (IIEST) (formerly Bengal Engineering and Science University), Shibpur, India, in 2003, the Master of Electrical Engineering degree from Jadavpur University, Kolkata, India, in 2006, and the Ph.D. degree from the Department of Electrical Engineering, Indian Institute of Technology (IIT), Kharagpur, India, in 2011. He is presently working as Associate Professor in the Department of Electronics and Electrical Engineering, IIT, Guwahati, India. His research interest includes distribution system planning and optimization, voltage control and stability, multi-objective optimization, custom power devices, hybrid energy systems, and evolutionary algorithms.